ACS APPLIED ELECTRONIC MATERIALS

pubs.acs.org/acsaelm Article

Photogated Synaptic Transistors Based on the Heterostructure of 4H-SiC and Organic Semiconductors for Neuromorphic Ultraviolet Vision

Xiao Liu, Wen Huang, Cuihong Kai, Lei Yin, Yue Wang, Xiaoping Liu, Xiaodong Pi,* and Deren Yang*

Cite This: ACS Appl. Electron. Mater. 2023, 5, 367−374 Read Online

ACCESS | Metrics & More | Article Recommendations | Supporting Information

ABSTRACT: Neuromorphic vision that integrates the functionalities of sensing, memory, and processing may provide an important approach to overcome the drawbacks of a conventional artificial visual system such as data redundancy and high-power consumption. It has exhibited considerable potential to mimic the functionalities of human vision even beyond the visible-light range. In this work, we show an ultraviolet (UV)-responsive synaptic transistor based on the heterostructure of 4H-SiC and organic semiconductors. Benefiting from the heterostructure design and photogating effect, the non-volatility of the synaptic transistor is achieved. Various biological synaptic functionalities are successfully mimicked by the synaptic transistor. The electrical energy consumption of the device per synaptic event is only 0.55 fJ, which is comparable to the energy consumption of a biological synapse. Furthermore, the dynamic learning and forgetting process of the image of a letter is simulated by using an array of the devices, demonstrating the potential of the UV-responsive synaptic devices for neuromorphic UV vision with the capability of the image recognition and memory.

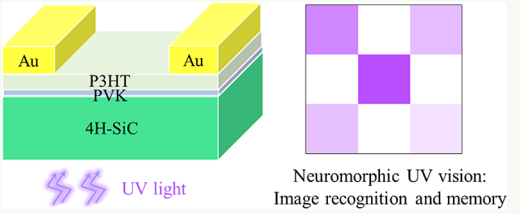

KEYWORDS: *neuromorphic vision, UV-responsive synaptic transistor, 4H-SiC/organic semiconductors, photogating, non-volatility*

INTRODUCTION

Relying on sensory neurons in a retina human vision is capable of parallelly sensing and processing visual information,[1] which has inspired research on artificial visual systems based on optoelectronic devices.[2,3] A conventional artificial visual system consists of a photoreceptive chip, an analog-to-digital converter, a memory unit, and a processing unit.[4] Such a system with physically separated functional units shows disadvantages of data redundancy, data access delay, and high power consumption.[5] In contrast, neuromorphic vision that is an artificial visual system based on non-volatile optoelectronic synaptic devices integrates the functionalities of sensing, memory, and processing. It may provide an important approach to overcome the drawbacks of a conventional artificial visual system. The neuromorphic vision has shown potential applications in image contrast enhancement,[1] image recognition,[5] pattern memory,[6] and so on.

The construction of neuromorphic vision increasingly requires UV-responsive synaptic devices.[6,7] Although a human retina cannot sense UV light, the majority of animal species use their UV vision for navigation, orientation, intraspecific communication, and food seeking.[8] For instance, bees use their excellent UV vision to distinguish flowers from complex surroundings and locate a nectar more easily.[9,10] Various materials such as Si nanocrystals,[11,12] organic semiconductors,[13,14] perovskite quantum dots,[15,16] two-dimensional materials,[17] and wide/ultrawide bandgap semiconductors[6,18−23] have been used to fabricate UV-responsive synaptic devices. As a typical wide-bandgap semiconductor, 4H-SiC is an ideal candidate for UV-responsive synaptic devices due to its intrinsic wide bandgap (3.3 eV), strong UV light absorption, UV radiation robustness,[24] and high thermal conductivity.[25] 4H-SiC has been already used in UV photodetectors,[26−28] position-dependent photodetectors,[29] and electronic synapses.[30]

In this work, a UV-responsive synaptic transistor based on the heterostructure of 4H-SiC and organic semiconductors is fabricated. The n-type 4H-SiC is used as the substrate and the main UV absorbing layer. The p-type organic materials are utilized because of their high hole carrier mobility[31] and widespread applications in optoelectronic synaptic devices.[13,32−34] The synaptic transistors show response to 375 nm UV light. Benefiting from the heterostructure design and photogating effect, the non-volatility of the synaptic transistors is achieved. Various biological synaptic functionalities such as the excitatory postsynaptic current (EPSC), paired-pulse facilitation (PPF), spike-duration-dependent plasticity (SDDP), spike-number-dependent plasticity (SNDP), spike-

Received: October 12, 2022
Accepted: December 30, 2022
Published: January 10, 2023

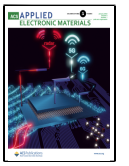

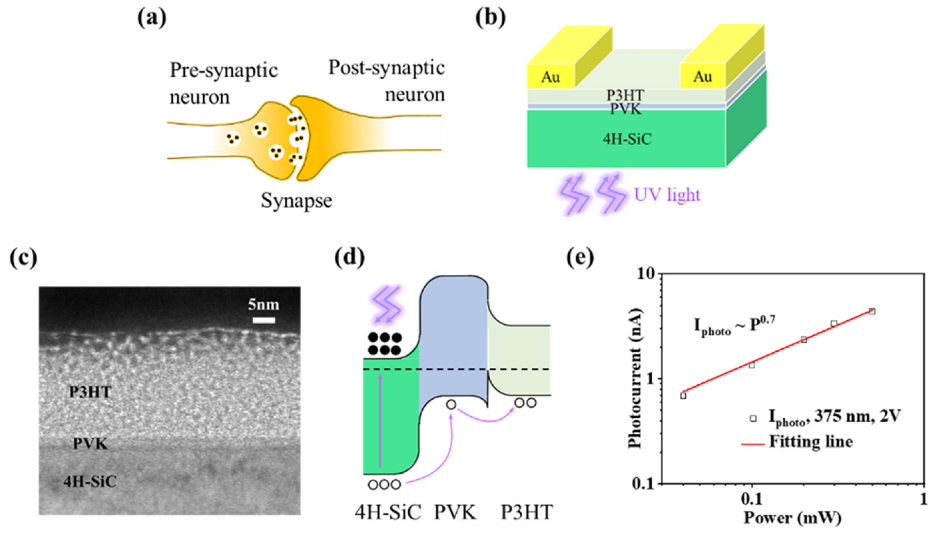

Figure 1. (a) Schematic representation of a biological synapse. (b) Schematic structure of the UV-responsive synaptic transistor. (c) Cross-sectional HRTEM image of the synaptic transistor. (d) Energy band diagram of 4H-SiC, PVK, and P3HT. (e) Photocurrent of the synaptic transistor as a function of the power of the 375 nm light.

rate-dependent plasticity (SRDP), and experiential learning are successfully mimicked by the synaptic transistors. Furthermore, the recognition and memory of an image of a letter are simulated by using an array of the devices.

EXPERIMENTAL SECTION

Materials and Device Fabrication. The heavily nitrogen (N)-doped 4H-SiC wafer with a thickness of 350 μm and a N concentration of 6×10^{18} to $1.5 \times 10^{19}/cm^3$ was purchased from TankeBlue Co., Ltd. The epitaxial 4H-SiC layer with a thickness of 10 μm was grown on the (0001) Si face of the wafer by hot wall chemical vapor deposition (HWCVD) (SICEP150A). The N concentration of the epitaxial 4H-SiC layer was $8.9 \times 10^{15}/cm^3$ obtained from capacitance-voltage measurements. In SiC, epitaxial growth is essential to produce active layers with designed doping density and thickness. The epitaxial 4H-SiC normally has low defect densities compared to the 4H-SiC substrate,[35] which is important for high-performance devices. In N-doped 4H-SiC, the minority carrier lifetime is inversely proportional to the majority carrier concentration.[36] The concentration of the free electrons in the lightly doped epitaxial 4H-SiC is about 2 orders of magnitude lower than that in the heavily doped 4H-SiC wafer,[37] which would dramatically reduce the recombination rate of the photogenerated holes.

The epitaxial wafer was cut into pieces of 10×10 mm^2. The small substrates were sequentially sonicated in acetone, ethanol, and deionized water for 5 min. They were then immersed in 30% H_2O_2 solution for 10 min and 5% HF solution for 5 min to remove any possible oxides on the surface. Afterward, the substrates were sonicated in deionized water for 5 min and dried with high-pressure N_2. To fabricate the 4H-SiC/PVK/P3HT devices, poly(9-vinylcarbazole) (PVK) (in mxylene, 10 mg/mL) was spin-coated on the substrate at a speed of 2000 rpm for 50 s and then annealed at 110 °C for 20 min. Poly(3-hexylthiophene) (P3HT) (in *o*-dichlorobenzene, 10 mg/mL) was subsequently spin-coated at a speed of 1000 rpm for 50 s and annealed at 130 °C for 20 min. For 4H-SiC/P3HT devices, P3HT was spin-coated directly on the 4H-SiC surface. Au electrodes (100 nm thick) were evaporated on the top of the P3HT film through a shadow mask, resulting in 25 μm long and 500 μm wide channels. UV glue was finally dropped on the channel area to encapsulate each device. The spin-coating of organic semiconductors, thermal evaporation of Au electrodes, and encapsulation of the devices were all performed in a glovebox.

Morphology Characterizations and Optoelectronic Measurements. Optical microscopy (AXIO IMAGER A2M, Zeiss) was used to attain the photograph (Figure S1a) of the synaptic transistor. Atomic force microscopy (AFM) (Dimension Edge, Bruker) was employed to investigate the morphology of the P3HT film on the 4H-SiC/PVK surface. The P3HT film surface is uniform with low roughness (Figure S1b). Scanning electronic microscopy (SEM) (Sigma300, Zeiss) and Fourier transform infrared spectroscopy (FTIR) (Is50, Thermo Fisher Scientific) were performed to investigate the thickness of the epitaxial 4H-SiC layer. A focused ion beam (FIB) system (FEI Quanta 3D FEG) was utilized to prepare a cross-sectional sample of a typical device. High-resolution transmission electron microscopy (HRTEM) (FEI Tecnai G2 F20) was employed to analyze the cross-sectional sample. The absorption spectra were measured by using a UV−vis−NIR spectrophotometer (UV-3600 Plus). Ultraviolet photoelectron spectroscopy (UPS) (Thermo Scientific ESCALAB 250Xi) was used to investigate the energy band structure of the epitaxial 4H-SiC. The optoelectronic measurements were performed with a Keithley 2450 SourceMeter. The synaptic functionalities were characterized by using a 375 nm laser. The light power density was measured with a power meter (Thorlabs GmbH, PM 100D). Optical spikes were generated with an optical shutter tuned by an arbitrary waveform generator (RIGOL DG4202). All the optoelectronic measurements were conducted in the ambient environment.

RESULTS AND DISCUSSION

The schematic structure of a biological synapse and the designed UV-responsive synaptic transistor are shown in Figure 1a and Figure 1b, respectively. The thickness of the epitaxial 4H-SiC (~10 μm) was obtained from the SEM image (Figure S2). In addition, FTIR was performed to analyze the thickness of the epitaxial 4H-SiC. Thickness values of 9.7309 ± 0.0156 μm were obtained after measuring five different points on the 4H-SiC surface, which are consistent with the SEM result. Thicknesses of the organic semiconductor layers (PVK: ~4 nm; P3HT: ~30 nm) were obtained from the cross-sectional HRTEM image (Figure 1c) of the synaptic transistor. Figure S3a shows the absorption spectra of PVK, P3HT, PVK/P3HT, 4H-SiC, 4H-SiC/P3HT, and 4H-SiC/PVK/P3HT samples in the wavelength range of 350−400 nm. Figure S3b shows the absorption spectra of PVK, P3HT, and PVK/P3HT samples in the wavelength range of 350−750 nm. It can be seen that the 375 nm UV light is mainly absorbed by the thick 4H-SiC layer, and the ultrathin PVK and P3HT films hardly

https://doi.org/10.1021/acsaelm.2c01390
ACS Appl. Electron. Mater. 2023, 5, 367−374

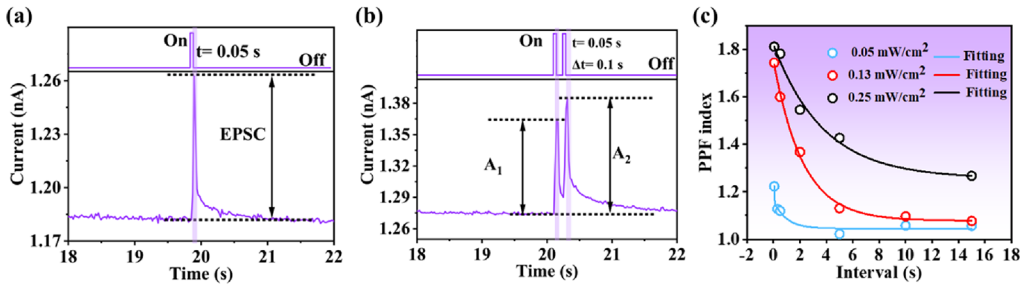

Figure 2. (a) EPSC of the synaptic transistor triggered by an optical spike (375 nm, 0.05 mW/cm^2, and 0.05 s). (b) EPSC of the synaptic transistor triggered by two consecutive optical spikes with a spike width of 0.05 s and spike interval (Δt) of 0.1 s. (c) Dependence of the PPF index on the interval of the two consecutive optical spikes. The external voltage applied on the device is 2 V during the measurements.

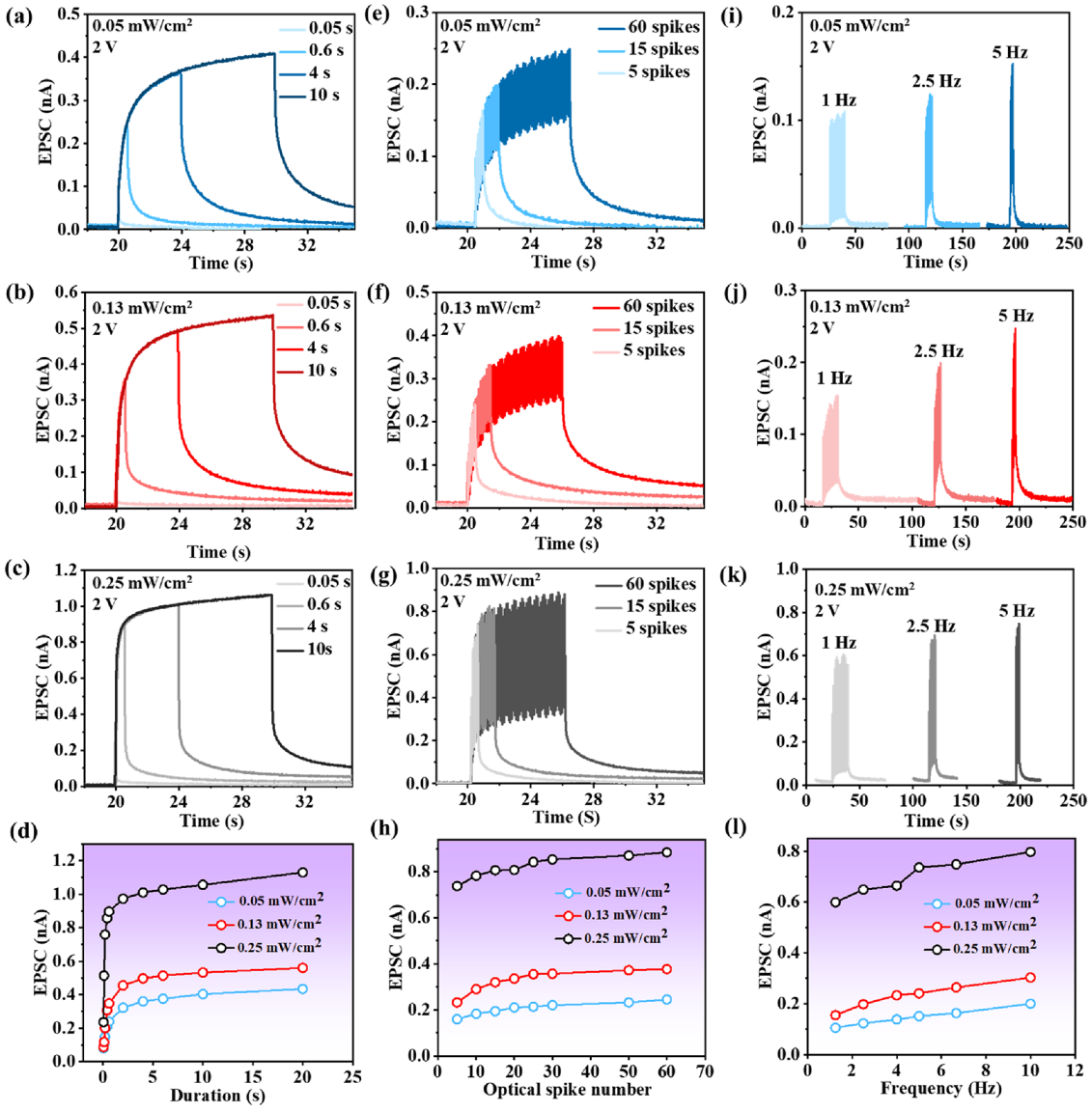

Figure 3. (a–c) Dependence of the EPSC triggered by an optical spike on the spike duration. (d) SDDP of the device. (e–g) Dependence of the EPSC on the optical spike number. The spike width and interval are both 0.05 s. (h) SNDP of the device. (i–k) Dependence of the EPSC triggered by 15 optical spikes on the spike frequency. The spike width is 0.05 s. (l) SRDP of the device.

absorb the UV light. The photogenerated carriers will be mainly generated in the 4H-SiC layer.

The energy band structure of the epitaxial 4H-SiC (−3.1, ∼ −3.5, and −6.4 eV) (conduction band, Fermi level, and valence band) (Figure S4) was investigated by using UPS under ultrahigh vacuum. The results agree well with that in the literature.[37,38] The energy band structures of PVK (−2.2, ∼ −5, and −5.8 eV)[39] and P3HT (−3.2, ∼ −4.4, and −5.2 eV)[40,41] (highest occupied molecular orbital (HOMO) level, Fermi level, and lowest unoccupied molecular orbital (LUMO)

https://doi.org/10.1021/acsaelm.2c01390
ACS Appl. Electron. Mater. 2023, 5, 367−374

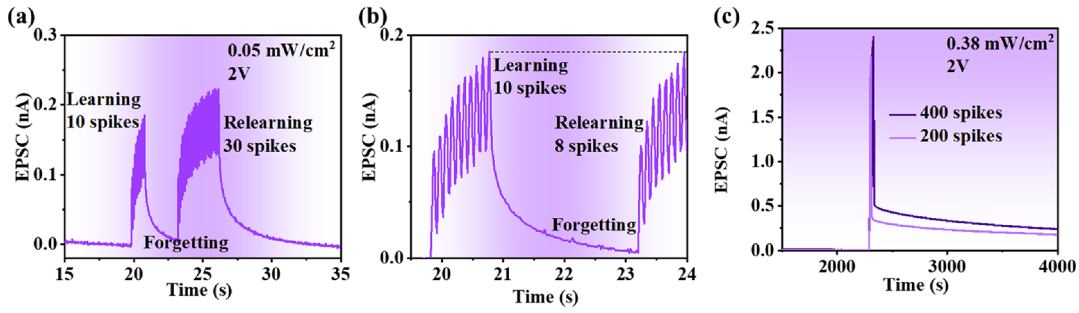

Figure 4. (a) Learning/forgetting/relearning process of the synaptic transistor. (b) Magnified view of panel (a). (c) EPSC of the synaptic transistor triggered by 200 and 400 optical spikes. The spike width and interval are both 0.05 s.

level) are obtained from the literature with the vacuum level (0 eV) as the reference level. As depicted in the energy band diagram (Figure 1d), PVK forms the p−n junction with 4H-SiC. The photogenerated electron−hole pairs in the 4H-SiC layer are separated immediately under the built-in electric field. Owing to the shallow LUMO level and deep HOMO level of PVK, the photogenerated electrons remain trapped in the 4H-SiC layer, while the photogenerated holes are transported and injected into the P3HT channel. Holes are responsible for the electrical conduction in the P3HT film. To validate the role of PVK as the electron blocking layer (EBL) and hole transport layer (HTL),[42,43] the decay curves of the normalized photocurrent stimulated by one optical spike (375 nm, 0.25 mW/cm^2, and 20 s) are compared for 4H-SiC/P3HT and 4H-SiC/PVK/P3HT devices (Figure S5). The decay time of the photocurrent increases from 0.6 to 1.5 s after the insertion of the PVK layer, affirming the critical role of PVK to elongate the lifetime of photogenerated holes in the P3HT channel and the achievement of the non-volatility of the synaptic transistor.

To gain further information on the conduction mechanism,[44] we studied the power dependency of the photocurrent of the synaptic transistor. The photocurrent generated in the device increases with the increase in the incident light power (Figure 1e). The data plotted in a log−log scale appears linear, which is a sign of a power law dependency. We fit the data to the equation $I_{photo} = A{\cdot}P^{\alpha}$, where I_{photo} is the net photocurrent, A is a constant, P is the light power, and α is a dimensionless fitting parameter.[45] Photoconductive and photogating effects have different power dependencies of the photocurrent: $\alpha = 1$ for the complete photoconductive effect and $\alpha < 1$ for the photogating effect.[45,46] The power exponent α is 0.7 for the synaptic transistor, indicating that there exists a photogating effect provided by the trapped photogenerated electrons in the 4H-SiC layer.[47] The hybrid-induced photogating effect modulates the conductance of the P3HT channel and induces a positive photocurrent, directly contributing to the non-volatility of the device,[47−50] which will be shown later.

The photogenerated holes here correspond to the neurotransmitters in a biological neural system. When neurotransmitters diffuse from the pre-synaptic membrane to the post-synaptic membrane, the EPSC is generated and the synaptic weight is strengthened. The EPSC of the synaptic transistor is triggered by an optical spike (375 nm, 0.05 mW/cm^2, and 0.05 s) (Figure 2a), indicating the increase in the channel conductivity. The modulation of the channel conductance by the photogating effect makes the synaptic transistor capable of mimicking various synaptic functionalities. PPF that is one of the important manifestations of short-term plasticity (STP) is demonstrated (Figure 2b). The PPF index is defined as A_2/A_1, where A_1 and A_2 are the EPSC values triggered by the first and second optical spike, respectively.[51] When the synaptic transistor is stimulated by the second optical spike, the photocurrent in the P3HT channel induced by the first optical spike has not decayed completely, leading to a higher A_2 than A_1. The PPF index decreases with the increase in the interval of the two consecutive optical spikes (Figure 2c), which is similar to the behavior of biological synapses.

In biological neural systems, while STP is related to the recognition and processing of input information that is forgettable, long-term plasticity (LTP) is associated with the formation of learning and memory that persist several hours or longer in the human brain.[52,53] The transition from STP to LTP can be achieved by enhancing stimulating intensity, duration, number, and frequency that persistently increase the synaptic weight.[1] Regarding the synaptic transistor, the STP-to-LTP transition can be realized by increasing light power density, spike duration, spike number, and spike frequency. Figure 3a−c shows the EPSC triggered by an optical spike as a function of the spike duration under three different light power densities (0.05, 0.13, and 0.25 mW/cm^2, respectively). A small EPSC triggered by a short spike (0.05 s) rapidly decays, while a larger EPSC triggered by a longer spike (10 s) decays much more slowly. The STP-to-LTP transition is also mimicked by increasing the optical spike number (Figure 3e−g) and spike frequency (Figure 3i−k) at different light power densities. It can be seen that the basic synaptic functionalities of a biological synapse such as SDDP (Figure 3d), SNDP (Figure 3h), and SRDP (Figure 3l) are successfully mimicked by our synaptic transistor. Figure S6 shows that the synaptic functionalities such as the EPSC, SDDP, SNDP, and SRDP can still be well emulated by the device after it has been stored in the glovebox for 6 months. The EPSC values of the device (Figure S6d−f) stimulated by identical optical spikes show no big difference from those of the as-prepared device, suggesting a relatively good long-term stability of the synaptic transistor.

"Experiential learning" that is one of the learning behaviors of biological neural systems is also mimicked by the synaptic transistor. As demonstrated in Figure 4a, when the synaptic transistor is stimulated by 10 optical spikes, the EPSC steadily increases. After the stimulation stops, the EPSC decreases, which is analogous to the forgetting process during the grasp of new knowledge of a human being.[54] When the synaptic transistor is stimulated by the optical spikes again, the maximum value of the previous EPSC is quickly reached within eight identical optical spikes (Figure 4b). During the "forgetting process", the EPSC stimulated by previous 10 optical spikes gradually decays to an intermediate value, meaning that there still exist some photogenerated holes in the

https://doi.org/10.1021/acsaelm.2c01390
ACS Appl. Electron. Mater. 2023, 5, 367−374

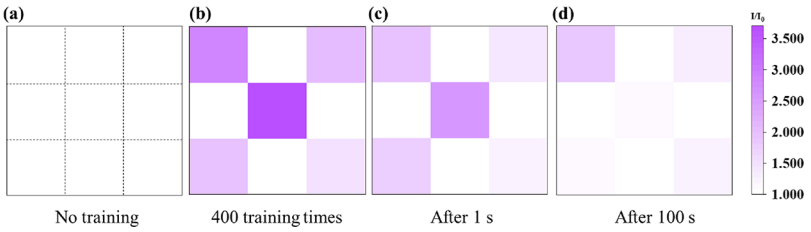

Figure 5. Dynamic learning and forgetting process of the image of the letter "X". I is the real-time current, while I_0 corresponds to the dark current of each device. The image obtained (a) without training, (b) after 400 training times (UV light stimulation: 375 nm, 0.38 mW/cm^2, 400 spikes with a spike width of 0.05 s and spike interval of 0.05 s, 2 V), (c) 1 s after the training, and (d) 100 s after the training.

Table 1. Comparison of the Electrical Energy Consumption of Different UV-Responsive Synaptic Devices

materials	wavelength(nm)	light powerdensity (mW/cm^2)	electrical energyconsumption (pJ)	reference
Si nanocrystals	375	1.3	940	11
C8-BTBT-C8/PAN	360	0.9	~420	13
C8-BTBT-C8	365	0.009	13.6	14
pentacene/PMMA/$CsPbBr_3$	365	0.041	~1.4 × 10^3	15
black phosphorus	280	0.4	3.5	17
ZnO NWs/sodium alginate	365	0.55	~1.1 × 10^3	6
InGaZnO/SiO_x	375	500	123	19
InGaZnO/Al_2O_3	365	3	~12.5	56
In_2O_3	365	0.91	~100	20
α-Ga_2O_3	254	0.005	1.1 × 10^{-2}	21
4H-SiC/PVK/P3HT	375	0.05	(5.5 ± 0.1) × 10^{-4}	this work

P3HT channel. Hence, less than 10 optical spikes are needed to reach the previous maximum EPSC, indicating that it is more efficient to relearn a previous forgotten knowledge than to learn for the first time.

The long-term retention capability (Figure S7a,b) of the synaptic transistor was also investigated by stimulating the device with 200 and 400 optical spikes (375 nm and 0.38 mW/cm^2). The EPSC does not decay completely even 10^4 s after the stimulation stops, proving the superior retention capability and the formation of long-term memory (LTM) of the synaptic transistor.

The magnified graphs of Figure S7a,b are organized in Figure 4c. Based on the LTM behavior, the simulation of the recognition and memory of a flower stamen image is shown as a proof of concept (Note S1 and Figure S8). In nature, most of the animals can sense UV light, which is of great significance for navigation, orientation, intraspecific communication, and food seeking.[8] Diverse flowers can reflect UV light to attract the nectarivorous pollinator with UV vision.[55] The UV-reflecting areas (shown in purple in Figure S8) positioned in the UV-absorbing parts (shown in black in Figure S8) display strong UV signals to help pollinators locate the floral nectar, while such signals are totally invisible to us humans that lack the UV photoreceptors in the retina.

By statistically investigating the LTM behavior of nine devices integrated in an array, the dynamic learning and forgetting process of the image of the letter "X" is demonstrated in Figure 5. The letter "X" is memorized in the array by selectively stimulating five devices with 400 optical spikes (375 nm, 0.38 mW/cm^2, a spike width of 0.05 s, and spike interval of 0.05 s, 2 V), indicating that a learning process is achieved (Figure 5b). The forgetting process is faster at the beginning (Figures 4c and 5c) followed by a slower process (Figure 5d). Even 100 s after the training, the letter "X" is still recognizable. The learning and forgetting behavior are consistent with those of the biological visual system, indicating the applications of the UV-responsive synaptic transistors in neuromorphic UV vision with the capability of the image recognition and memory.

Low energy consumption is critical for neuromorphic UV vision. Figure S7c shows one typical current curve of a single synaptic event triggered by one optical spike (375 nm, 0.05 mW/cm^2, 0.0005 V, and 0.02 s). According to eq S1 described in Note S2, the average energy consumption of a single synaptic event calculated from three independent measurements is only 0.55 fJ. The energy consumption is lower than that of other UV-responsive synaptic devices based on Si nanocrystals,[11] organic semiconductors,[13,14] perovskite quantum dots,[15] two-dimensional materials,[17] other wide-bandgap materials,[6,19,56] and ultrawide bandgap materials[21] in the literature (Table 1). The energy consumption is also comparable to that of a biological synapse (1−100 fJ).[57]

CONCLUSIONS

In summary, we have shown a UV-responsive synaptic transistor based on the heterostructure of 4H-SiC and organic semiconductors. Benefiting from the device structure design and photogating effect, the non-volatility of the synaptic transistor has been achieved. Various synaptic functionalities such as the EPSC, PPF, SDDP, SNDP, SRDP, and experiential learning have been mimicked by the synaptic transistor. The device shows superior retention capability with duration of the photocurrent beyond 10^4 s after the stimulation of repeating optical spikes. The electrical energy consumption of the device per synaptic event is only 0.55 fJ, which is lower than that of other UV-responsive synaptic devices. In addition, the dynamic learning and forgetting process of the image of a letter is simulated by using an array of the devices, demonstrating the potential of the UV-responsive synaptic devices for neuromorphic UV vision with the capability of image recognition and memory.

https://doi.org/10.1021/acsaelm.2c01390
ACS Appl. Electron. Mater. 2023, 5, 367−374

■ ASSOCIATED CONTENT

Supporting Information

The Supporting Information is available free of charge at https://pubs.acs.org/doi/10.1021/acsaelm.2c01390.

Additional notes, figures, and equations including the photograph of the 4H-SiC/organic semiconductor-based synaptic transistor, SEM image of the ~10 μm-thick epitaxial 4H-SiC layer, absorption spectra, etc (PDF)

■ AUTHOR INFORMATION

Corresponding Authors

Xiaodong Pi − *State Key Laboratory of Silicon Materials & School of Materials Science Engineering, Zhejiang University, Hangzhou, Zhejiang 310027, China; Institute of Advanced Semiconductors & Zhejiang Provincial Key Laboratory of Power Semiconductor Materials and Devices, Hangzhou Innovation Center, Zhejiang University, Hangzhou, Zhejiang 311200, China;* orcid.org/0000-0002-4233-6181; Email: xdpi@zju.edu.cn

Deren Yang − *State Key Laboratory of Silicon Materials & School of Materials Science Engineering, Zhejiang University, Hangzhou, Zhejiang 310027, China; Institute of Advanced Semiconductors & Zhejiang Provincial Key Laboratory of Power Semiconductor Materials and Devices, Hangzhou Innovation Center, Zhejiang University, Hangzhou, Zhejiang 311200, China*; Email: mseyang@zju.edu.cn

Authors

Xiao Liu − *State Key Laboratory of Silicon Materials & School of Materials Science Engineering, Zhejiang University, Hangzhou, Zhejiang 310027, China; Institute of Advanced Semiconductors & Zhejiang Provincial Key Laboratory of Power Semiconductor Materials and Devices, Hangzhou Innovation Center, Zhejiang University, Hangzhou, Zhejiang 311200, China;* orcid.org/0000-0001-7678-6570

Wen Huang − *New Energy Technology Engineering Laboratory of Jiangsu Provence and School of Science, Nanjing University of Posts and Telecommunications, Nanjing 210023, China*

Cuihong Kai − *State Key Laboratory of Silicon Materials & School of Materials Science Engineering, Zhejiang University, Hangzhou, Zhejiang 310027, China; Institute of Advanced Semiconductors & Zhejiang Provincial Key Laboratory of Power Semiconductor Materials and Devices, Hangzhou Innovation Center, Zhejiang University, Hangzhou, Zhejiang 311200, China*

Lei Yin − *State Key Laboratory of Silicon Materials & School of Materials Science Engineering, Zhejiang University, Hangzhou, Zhejiang 310027, China*

Yue Wang − *State Key Laboratory of Silicon Materials & School of Materials Science Engineering, Zhejiang University, Hangzhou, Zhejiang 310027, China; Institute of Advanced Semiconductors & Zhejiang Provincial Key Laboratory of Power Semiconductor Materials and Devices, Hangzhou Innovation Center, Zhejiang University, Hangzhou, Zhejiang 311200, China*

Xiaoping Liu − *Institute of Advanced Semiconductors & Zhejiang Provincial Key Laboratory of Power Semiconductor Materials and Devices, Hangzhou Innovation Center, Zhejiang University, Hangzhou, Zhejiang 311200, China*

Complete contact information is available at: https://pubs.acs.org/10.1021/acsaelm.2c01390

Notes

The authors declare no competing financial interest.

■ ACKNOWLEDGMENTS

This work is supported by the National Key Research and Development Program of China (grant no. 2018YFB2200101), Natural Science Foundation of China (grant nos. 91964107, U20A20209, 62104114, and U22A2075), and the "Pioneer" and "Leading Goose" R&D Program of Zhejiang (grant no. 2022C01021). Partial support is provided by the Natural Science Foundation of China for Innovative Research Groups (grant no. 61721005), the Fundamental Research Funds for the Central Universities (grant no. 226-2022-00200), the Natural Science Foundation of Jiangsu Province (grant no. BK20200760), and the Introduction of Talents Project of Nanjing University of Posts and Telecommunications (grant no. NY220097).

■ REFERENCES

(1) Zhou, F.; Zhou, Z.; Chen, J.; Choy, T. H.; Wang, J.; Zhang, N.; Lin, Z.; Yu, S.; Kang, J.; Wong, H.-S. P.; Chai, Y. Optoelectronic Resistive Random Access Memory for Neuromorphic Vision Sensors. *Nat. Nanotechnol.* **2019**, *14*, 776−782.

(2) Liao, F.; Zhou, F.; Chai, Y. Neuromorphic Vision Sensors: Principle, Progress and Perspectives. *J. Semicond.* **2021**, *42*, 13105.

(3) Wen, W.; Guo, Y.; Liu, Y. Multifunctional Neurosynaptic Devices for Human Perception Systems. *J. Semicond.* **2022**, *43*, No. 051201.

(4) Zhou, F.; Chai, Y. Near-Sensor and in-Sensor Computing. *Nat. Electron.* **2020**, *3*, 664−671.

(5) Li, G.; Xie, D.; Zhong, H.; Zhang, Z.; Fu, X.; Zhou, Q.; Li, Q.; Ni, H.; Wang, J.; Guo, E.; He, M.; Wang, C.; Yang, G.; Jin, K.; Ge, C. Photo-Induced Non-Volatile VO2 Phase Transition for Neuromorphic Ultraviolet Sensors. *Nat. Commun.* **2022**, *13*, 1729.

(6) Sun, F.; Lu, Q.; Liu, L.; Li, L.; Wang, Y.; Hao, M.; Cao, Z.; Wang, Z.; Wang, S.; Li, T.; Zhang, T. Bioinspired Flexible, Dual-Modulation Synaptic Transistors toward Artificial Visual Memory Systems. *Adv. Mater. Technol.* **2020**, *5*, No. 1900888.

(7) Park, H.-L.; Kim, H.; Lim, D.; Zhou, H.; Kim, Y.-H.; Lee, Y.; Park, S.; Lee, T.-W. Retina-Inspired Carbon Nitride-Based Photonic Synapses for Selective Detection of UV Light. *Adv. Mater.* **2020**, *32*, No. 1906899.

(8) Cronin, T. W.; Bok, M. J. Photoreception and Vision in the Ultraviolet. *J. Exp. Biol.* **2016**, *219*, 2790−2801.

(9) Chittka, L.; Shmida, A.; Troje, N.; Menzel, R. Ultraviolet as a Component of Flower Reflections, and the Colour Perception of Hymenoptera. *Vis. Res.* **1994**, *34*, 1489−1508.

(10) Kevan, P. G.; Chittka, L.; Dyer, A. G. Limits to the Salience of Ultraviolet: Lessons from Colour Vision in Bees and Birds. *J. Exp. Biol.* **2001**, *204*, 2571−2580.

(11) Yin, L.; Han, C.; Zhang, Q.; Ni, Z.; Zhao, S.; Wang, K.; Li, D.; Xu, M.; Wu, H.; Pi, X.; Yang, D. Synaptic Silicon-Nanocrystal Phototransistors for Neuromorphic Computing. *Nano Energy* **2019**, *63*, No. 103859.

(12) Bu, M.; Wang, Y.; Yin, L.; Tong, Z.; Zhang, Y.; Yang, D.; Pi, X. Synaptic Devices Based on Semiconductor Nanocrystals. *Front. Info. Technol. Electron. Eng.* **2022**, 1579.

(13) Dai, S.; Wu, X.; Liu, D.; Chu, Y.; Wang, K.; Yang, B.; Huang, J. Light-Stimulated Synaptic Devices Utilizing Interfacial Effect of Organic Field-Effect Transistors. *ACS Appl. Mater. Interfaces* **2018**, *10*, 21472−21480.

(14) Yang, C.; Qian, J.; Jiang, S.; Wang, H.; Wang, Q.; Wan, Q.; Chan, P. K. L.; Shi, Y.; Li, Y. An Optically Modulated Organic Schottky-Barrier Planar-Diode-Based Artificial Synapse. *Adv. Opt. Mater.* **2020**, *8*, No. 2000153.

(15) Wang, Y.; Lv, Z.; Chen, J.; Wang, Z.; Zhou, Y.; Zhou, L.; Chen, X.; Han, S.-T. Photonic Synapses Based on Inorganic Perovskite

Quantum Dots for Neuromorphic Computing. *Adv. Mater.* **2018**, *30*, No. 1802883.
(16) Chen, S.; Huang, J. Recent Advances in Synaptic Devices Based on Halide Perovskite. *ACS Appl. Electron. Mater.* **2020**, *2*, 1815−1825.
(17) Ahmed, T.; Kuriakose, S.; Mayes, E. L. H.; Ramanathan, R.; Bansal, V.; Bhaskaran, M.; Sriram, S.; Walia, S. Optically Stimulated Artificial Synapse Based on Layered Black Phosphorus. *Small* **2019**, *15*, No. 1900966.
(18) Lee, M.; Nam, S.; Cho, B.; Kwon, O.; Lee, H. U.; Hahm, M. G.; Kim, U. J.; Son, H. Accelerated Learning in Wide-Band-Gap AlN Artificial Photonic Synaptic Devices: Impact on Suppressed Shallow Trap Level. *Nano Lett.* **2021**, *21*, 7879−7886.
(19) Duan, N.; Li, Y.; Chiang, H.-C.; Chen, J.; Pan, W.-Q.; Zhou, Y.-X.; Chien, Y.-C.; He, Y.-H.; Xue, K.-H.; Liu, G.; Chang, T.-C.; Miao, X.-S. An Electro-Photo-Sensitive Synaptic Transistor for Edge Neuromorphic Visual Systems. *Nanoscale* **2019**, *11*, 17590−17599.
(20) Alquraishi, W.; Fu, Y.; Qiu, W.; Wang, J.; Chen, Y.; Kong, L.-A.; Sun, J.; Gao, Y. Hybrid Optoelectronic Synaptic Functionality Realized with Ion Gel-Modulated In2O3 Phototransistors. *Org. Electron.* **2019**, *71*, 72−78.
(21) Zhu, R.; Liang, H.; Hu, S.; Wang, Y.; Mei, Z. Amorphous-Ga2O3 Optoelectronic Synapses with Ultra-Low Energy Consumption. *Adv. Electron. Mater.* **2022**, *8*, No. 2100741.
(22) Jiang, D.; Li, J.; Fu, W.; Chen, Q.; Yang, Y.; Zhou, Y.; Zhang, J. Light-Stimulated Artificial Synapse with Memory and Learning Functions by Utilizing an Aqueous Solution-Processed In2O3/AlLiO Thin-Film Transistor. *ACS Appl. Electron. Mater.* **2020**, *2*, 2772−2779.
(23) Peng, C.; Jiang, W.; Li, Y.; Li, X.; Zhang, J. Photoelectric IGZO Electric-Double-Layer Transparent Artificial Synapses for Emotional State Simulation. *ACS Appl. Electron. Mater.* **2019**, *1*, 2406−2414.
(24) Prasai, D.; John, W.; Weixelbaum, L.; Krüger, O.; Wagner, G.; Sperfeld, P.; Nowy, S.; Friedrich, D.; Winter, S.; Weiss, T. Highly Reliable Silicon Carbide Photodiodes for Visible-Blind Ultraviolet Detector Applications. *J. Mater. Res.* **2013**, *28*, 33−37.
(25) Karanth, S. P.; Sumesh, M. A.; Shobha, V.; Sirisha, J.; Yadav, M. D.; Vijay, S. B.; Sriram, K. V. Electro-Optical Performance Study of 4H-SiC/Pd Schottky UV Photodetector Array for Space Applications. *IEEE Trans. Electron Devices* **2020**, *67*, 3242−3249.
(26) Aldalbahi, A.; Li, E.; Rivera, M.; Velazquez, R.; Altalhi, T.; Peng, X.; Feng, P. X. A New Approach for Fabrications of SiC Based Photodetectors. *Sci. Rep.* **2016**, *6*, 23457.
(27) Yu, J.; Dong, L.; Peng, B.; Yuan, L.; Huang, Y.; Zhang, L.; Zhang, Y.; Jia, R. Self-Powered Photodetectors Based on β-Ga2O3/4H−SiC Heterojunction with Ultrahigh Current on/off Ratio and Fast Response. *J. Alloys Compd.* **2020**, *821*, No. 153532.
(28) Zhang, Y.; Wang, Y.; Wang, L.; Zhu, L.; Wang, Z. L. Highly Sensitive Photoelectric Detection and Imaging Enhanced by the Pyro-Phototronic Effect Based on a Photoinduced Dynamic Schottky Effect in 4H-SiC. *Adv. Mater.* **2022**, *34*, No. 2204363.
(29) Sarker, B. K.; Cazalas, E.; Chung, T.-F.; Childres, I.; Jovanovic, I.; Chen, Y. P. Position-Dependent and Millimetre-Range Photodetection in Phototransistors with Micrometre-Scale Graphene on SiC. *Nat. Nanotechnol.* **2017**, *12*, 668−674.
(30) Liu, L.; Zhao, J.; Cao, G.; Zheng, S.; Yan, X. A Memristor-Based Silicon Carbide for Artificial Nociceptor and Neuromorphic Computing. *Adv. Mater. Technol.* **2021**, *6*, No. 2100373.
(31) Janasz, L.; Chlebosz, D.; Gradzka, M.; Zajaczkowski, W.; Marszalek, T.; Müllen, K.; Ulanski, J.; Kiersnowski, A.; Pisula, W. Improved Charge Carrier Transport in Ultrathin Poly(3-Hexylthiophene) Films via Solution Aggregation. *J. Mater. Chem. C* **2016**, *4*, 11488−11498.
(32) Li, Y.; Wang, Y.; Yin, L.; Huang, W.; Peng, W.; Zhu, Y.; Wang, K.; Yang, D.; Pi, X. Silicon-Based Inorganic-Organic Hybrid Optoelectronic Synaptic Devices Simulating Cross-Modal Learning. *Sci. China Info. Sci.* **2021**, *64*, 162401.
(33) Wang, Y.; Zhu, Y.; Li, Y.; Zhang, Y.; Yang, D.; Pi, X. Dual-Modal Optoelectronic Synaptic Devices with Versatile Synaptic Plasticity. *Adv. Funct. Mater.* **2022**, *32*, No. 2107973.
(34) Yang, W.-C.; Lin, Y.-C.; Inagaki, S.; Shimizu, H.; Ercan, E.; Hsu, L.-C.; Chueh, C.-C.; Higashihara, T.; Chen, W.-C. Low-Energy-Consumption and Electret-Free Photosynaptic Transistor Utilizing Poly(3-Hexylthiophene)-Based Conjugated Block Copolymers. *Adv. Sci.* **2022**, *9*, No. 2105190.
(35) Hao, D.; Zhang, J.; Dai, S.; Zhang, J.; Huang, J. Perovskite/Organic Semiconductor-Based Photonic Synaptic Transistor for Artificial Visual System. *ACS Appl. Mater. Interfaces* **2020**, *12*, 39487−39495.
(36) Yu, J. Y.; Yang, X. L.; Peng, Y.; Chen, X. F.; Hu, X. B.; Xu, X. G. Inhomogeneity of Minority Carrier Lifetime in 4H-SiC Substrates. *Crystallogr. Rep.* **2020**, *65*, 1231−1236.
(37) Kimoto, T.; Cooper, J. A. Physical Properties of Silicon Carbide. In *Fundamentals of Silicon Carbide Technology*; John Wiley & Sons, Ltd, 2014; pp. 11−38.
(38) Jia, L.; Zheng, W.; Lin, R.; Huang, F. Ultra-High Photovoltage (2.45 V) Forming in Graphene Heterojunction via Quasi-Fermi Level Splitting Enhanced Effect. *iScience* **2020**, *23*, No. 100818.
(39) Guo, X.; Liu, X.; Lin, F.; Li, H.; Fan, Y.; Zhang, N. Highly Conductive Transparent Organic Electrodes with Multilayer Structures for Rigid and Flexible Optoelectronics. *Sci. Rep.* **2015**, *5*, 10569.
(40) Dietmueller, R.; Nesswetter, H.; Schoell, S. J.; Sharp, I. D.; Stutzmann, M. Band Alignment at Organic−Inorganic Heterojunctions between P3HT and n-Type 6H-SiC. *ACS Appl. Mater. Interfaces* **2011**, *3*, 4286−4291.
(41) Zhao, S.; Wang, Y.; Huang, W.; Jin, H.; Huang, P.; Wang, H.; Wang, K.; Li, D.; Xu, M.; Yang, D.; Pi, X. Developing Near-Infrared Quantum-Dot Light-Emitting Diodes to Mimic Synaptic Plasticity. *Sci. China Mater.* **2019**, *62*, 1470−1478.
(42) Ho, M. D.; Kim, D.; Kim, N.; Cho, S. M.; Chae, H. Polymer and Small Molecule Mixture for Organic Hole Transport Layers in Quantum Dot Light-Emitting Diodes. *ACS Appl. Mater. Interfaces* **2013**, *5*, 12369−12374.
(43) Liu, X.; Zhao, S.; Gu, W.; Zhang, Y.; Qiao, X.; Ni, Z.; Pi, X.; Yang, D. Light-Emitting Diodes Based on Colloidal Silicon Quantum Dots with Octyl and Phenylpropyl Ligands. *ACS Appl. Mater. Interfaces* **2018**, *10*, 5959−5966.
(44) Tong, X. W.; Zhang, Z. X.; Wang, D.; Luo, L. B.; Xie, C.; Wu, Y. C. Inorganic CsBi 3 I 10 Perovskite/Silicon Heterojunctions for Sensitive, Self-Driven and Air-Stable NIR Photodetectors. *J. Mater. Chem. C* **2019**, *7*, 863−870.
(45) Li, L.; Wang, W.; Chai, Y.; Li, H.; Tian, M.; Zhai, T. Few-Layered PtS2 Phototransistor on h-BN with High Gain. *Adv. Funct. Mater.* **2017**, *27*, 1−8.
(46) Island, J. O.; Blanter, S. I.; Buscema, M.; Van Der Zant, H. S. J.; Castellanos-Gomez, A. Gate Controlled Photocurrent Generation Mechanisms in High-Gain In2Se3 Phototransistors. *Nano Lett.* **2015**, *15*, 7853−7858.
(47) Sazali, E. S.; Sahar, M. R.; Ghoshal, S. K. Device Applications of Band-Structure-Engineered Nanomaterials Current Status and Future Trend. *Int. J. Nanoelectron. Mater.* **2015**, *8*, 129−202.
(48) Tao, J.; Sanchez Vazquez, J.; Chae, H. U.; Ahsan, R.; Kapadia, R. Machine Vision With InP Based Floating-Gate Photo-Field-Effective Transistors for Color-Mixed Image Recognition. *IEEE J. Quantum Electron.* **2022**, *58*, 1.
(49) Fang, H.; Hu, W. Photogating in Low Dimensional Photodetectors. *Adv. Sci.* **2017**, *4*, No. 1700323.
(50) Zhai, Y.; Zhou, Y.; Yang, X.; Wang, F.; Ye, W.; Zhu, X.; She, D.; Lu, W. D.; Han, S. T. Near Infrared Neuromorphic Computing via Upconversion-Mediated Optogenetics. *Nano Energy* **2020**, *67*, No. 104262.
(51) Zucker, R. S.; Regehr, W. G. Short-Term Synaptic Plasticity. *Annu. Rev. Physiol.* **2002**, *64*, 355−405.
(52) Abbott, L. F.; Regehr, W. G. Synaptic Computation. *Nature* **2004**, *431*, 796−803.
(53) Wang, Y.; Yin, L.; Huang, W.; Li, Y.; Huang, S.; Zhu, Y.; Yang, D.; Pi, X. Optoelectronic Synaptic Devices for Neuromorphic Computing. *Adv. Intel. Syst.* **2021**, *3*, No. 2000099.

(54) Ebbinghaus, H. Memory: A Contribution to Experimental Psychology. *Ann. Neurosci.* **2013**, *20*, 155−156.
(55) Lunau, K.; Ren, Z.-X.; Fan, X.-Q.; Trunschke, J.; Pyke, G. H.; Wang, H. Nectar Mimicry: A New Phenomenon. *Sci. Rep.* **2020**, *10*, 7039.
(56) Li, H. K.; Chen, T. P.; Liu, P.; Hu, S. G.; Liu, Y.; Zhang, Q.; Lee, P. S. A Light-Stimulated Synaptic Transistor with Synaptic Plasticity and Memory Functions Based on InGaZnOx−Al2O3 Thin Film Structure. *J. Appl. Phys.* **2016**, *119*, 244505.
(57) van de Burgt, Y.; Lubberman, E.; Fuller, E. J.; Keene, S. T.; Faria, G. C.; Agarwal, S.; Marinella, M. J.; Alec Talin, A.; Salleo, A. A Non-Volatile Organic Electrochemical Device as a Low-Voltage Artificial Synapse for Neuromorphic Computing. *Nat. Mater.* **2017**, *16*, 414−418.

https://doi.org/10.1021/acsaelm.2c01390
ACS Appl. Electron. Mater. 2023, 5, 367−374